# A high-resolution subcellular map of proteins in ciliated cells

*Filippa Bertilsson[1], Feria Hikmet[1], Jan N. Hansen[2,3], Mathias Uhlén[2,4], Loren Méar[1,5,6]†, Cecilia Lindskog[1]†**

*†These authors contributed equally*

[1] Department of Immunology, Genetics and Pathology, Cancer Precision Medicine Research Unit, Uppsala University, SE-75185 Uppsala, Sweden

[2] Science for Life Laboratory, School of Engineering Sciences in Chemistry, Biotechnology and Health, KTH Royal Institute of Technology, 17121 Stockholm, Sweden

[3] Department of Bioengineering, Stanford University, Stanford, CA, USA

[4] Department of Neuroscience, Karolinska Institutet, Stockholm, Sweden

[5] Department of Women's and Children's Health, Karolinska Institutet, 17177 Stockholm, Sweden

[6] Department of Gynaecology and Reproductive Medicine, Karolinska University Hospital, Stockholm, Sweden

KEYWORDS

Antibody-based proteomics, Human Protein Atlas, Motile cilia, Ciliated cells, multiplex immunohistochemistry, image analysis, protein mapping

**Abstract**

Motile cilia are complex structures regulated by thousands of genes, essential for various physiological functions like respiration and reproduction. Their dysfunction can result in severe conditions like primary ciliary dyskinesia (PCD), highlighting the need for a deeper molecular understanding of their specific ciliary compartments. Interestingly, ciliated cells harbor multiple proteins with limited evidence on biological function, as defined by Functional Evidence (FE) scores, a grading system developed by the Human Proteome Project (HPP). Building upon the stringent antibody validation pipeline of the Human Protein Atlas (HPA) project, we developed a high-throughput workflow that combines a novel multiplex immunohistochemistry protocol with image analysis to investigate protein expression and subcellular localization in motile ciliated cells across five human tissues: nasopharynx, bronchus, Fallopian tube, endometrium, and cervix. We spatially mapped >180 proteins, out of which 73% have FE scores 2-5, suggesting that further evidence is needed to establish these proteins' biological function. Notably expression patterns varied between tissues, suggesting that motile cilia proteins are not universally expressed across the different epithelia. Our pipeline constitutes a promising resource for comprehensive mapping of the motile cilia proteome, and a first step towards identifying cilia proteins for functional studies to understand the molecular mechanisms underlying ciliopathies.

## Introduction

Cells are not organized randomly, but instead form complex organ systems where molecules, cellular compartments and cell types are spatially distributed based on cellular function. Proteins often execute their functions in specific subcellular locations, which is crucial for maintaining various cellular processes such as cell growth, motility, and signaling(*1*). To investigate the role of proteins and their biochemical functions within the cell, knowledge about the spatial localization from both a cellular and subcellular perspective is a crucial first step for further functional studies(*2*).

The Human Proteome Project (HPP) is an initiative of the Human Proteome Organization (HUPO) that has contributed to credibly identifying at least one major isoform of all human proteins, mainly using mass spectrometry-based methods (*3*). As a next step, the HPP consortium currently leads a major effort called the "Grand Challenge", with the ultimate goal to gain a solid understanding of at least one biological function for each protein at the molecular level. A Functional Evidence (FE) scoring system has been developed, with FE1-5 elucidating the amount of evidence for protein function. FE5 represents the lowest scoring, indicating that basically nothing is known about the role of these proteins in human cells.

With the goal of mapping all human proteins, the Human Protein Atlas (HPA) project has built one of the world's largest biological knowledge resources, available as an open-access database (www.proteinatlas.org). The HPA integrates both transcriptomics data and spatial antibody-based proteomics(*4*), and within this effort, >15,000 proteins have been mapped to all major human normal and cancer tissues using classical immunohistochemistry (IHC). The resource of more than 10 million manually annotated high-resolution histological images provides important information

on spatial expression patterns of proteins from a body-wide and cell type-specific perspective, but the possibilities to distinguish subcellular patterns are limited.

IHC is primarily used to study one protein at a time, but an increasing number of methods utilize multiplexed IHC (mIHC), enabling novel insights into co-expression and tissue or cell type heterogeneity. Spatial proteomics technologies are of utmost importance to characterize the intrinsic subcellular functions of human proteins(*5*), as has been demonstrated in multiple large-scale studies(*2*, *6*). To increase the resolution of the Tissue resource in the HPA, the most recent update of the HPA (HPAv24) includes data based on a novel mIHC protocol employing 6-plex in-house generated antibody panels. Using an iterative fluorescence-based staining-stripping method, fixed antibody panels of five markers outlining specific cell types, cell states or subcellular structures were stained together with proteins of interest. By examining overlap in expression, this workflow allows for exploring protein localization in structures that are challenging to distinguish based on histological examination only. This facilitates automated image analyses efforts, and minimizes the subjectivity introduced during manual annotation(*6*, *7*).

Interestingly, when comparing the FE scores with single cell type specificity in the HPA, a dataset based on single-cell transcriptomics(*8*), as many as 441 proteins with FE2-5 showed an elevated expression in ciliated cells. This suggests that further mapping of these cells is an important contribution towards understanding protein function. Here, we therefore seek to further explore the cilium (plural cilia), a filamentous hair-like cellular membrane protrusion, whose assembly (ciliogenesis) and structure requires at least 2,000 genes(*9*). Cilia are canonically distinguished into two types: primary cilia and motile cilia. Motile cilia are present on epithelia of different organs where they aid in transporting cells, fluids, particles or mucus, and are crucial for e.g. reproduction, respiration, L/R body asymmetry, or brain development and function(*10*). Defects

in genes related to motile cilia have been linked to motile ciliopathies, contributing to a large spectrum of diseases in various tissues, including chronic respiratory problems, infertility, and hydrocephalus(*11*). The most common ciliopathy, primary ciliary dyskinesia (PCD), is characterized by impaired ciliary movement. PCD is usually caused by autosomal recessive mutations, but also by autosomal dominant and even X-linked mutations in rare cases(*12*, *13*).

Despite advancements in understanding PCD in the last 20 years, its diagnosis remains challenging, and effective treatments are lacking(*14*). Studying motile cilia genes can provide us with fundamental insights into ciliary function and structure, being a first step towards understanding the underlying molecular mechanisms of ciliopathies (e.g., impaired mucociliary clearance in the airways)(*15*). Structurally, the cilium comprises several distinct regions: the rootlet, which anchors the cilium to the cell and serves as a microtubule organizing center; the transition zone, a specialized gateway at the ciliary base that regulates protein trafficking and acts as a diffusion barrier; and the axoneme, the core ciliary skeleton that extends from the centrioles in the rootlet and traverses the transition zone and that is composed of microtubule doublets and associated motor proteins that mediate ciliary movement(*16*, *17*). Given their small size, close spatial proximity, and dynamic nature, these compartments are best studied for their architecture using imaging and microscopy-based methods(*18*). To our knowledge, no previous mIHC panel exists that enables detailed characterization of the different sub-compartments of ciliated cells at a high resolution. Therefore, we developed a medium-plex mIHC panel specifically designed to map motile cilia architecture.

With this background, the aim of the study was to develop a novel high-throughput workflow for quantifying cilia proteins at subcellular resolution using mIHC and automated image analysis, a first step towards understanding protein function. Based on signal overlap with a panel of marker proteins outlining the cilium, the transition zone, the rootlet, the cytoplasm, and the nucleus of ciliated cells, the spatial subcellular localization of 187 motile cilia proteins was mapped across five different tissue types from both respiratory (nasopharynx and bronchus) and reproductive tracts (fallopian tube, endometrium and cervix). The detailed information at the tissue, cellular, and subcellular levels offered new insights into the presumed functions of these proteins in motile cilia. Moreover, our approach, combining spatial proteomics with automated image analysis enables detailed spatial mapping at the subcellular level, offering a valuable resource for future large-scale studies of cilia biology in health and disease. The resulting images can be explored in the open access Human Protein Atlas (www.proteinatlas.org).

## Results

### *Development of a multiplex panel for motile ciliated cells*

In this project, a multiplex immunohistochemistry (mIHC) panel was developed with the goal to study the subcellular localization of proteins to the different subcellular structures of ciliated cells across different tissue types (Figure 1A). A list of 187 protein candidates relevant for further exploration with reliable expression patterns in motile ciliated cells was compiled based on IHC and mRNA data in the Human Protein Atlas (www.proteinatlas.org) database(*4*). A dedicated tissue microarray (TMA) was created, including five tissue types known to harbor motile ciliated cells in both the respiratory and reproductive tracts: nasopharynx (N), bronchus (B), fallopian tube

(FT), endometrium (E), and cervix (C) (Figure 1B; Supplementary Table 1). To precisely determine the localization of candidate proteins using an iterative mIHC workflow, a fixed panel of five antibodies outlining different subcellular structures of motile ciliated cells was developed (Figure 1C). The panel was combined with one antibody for a new candidate protein per slide (Figure 1D). This design allowed for a standardized high-throughput characterization of subcellular protein localization across multiple tissue samples.

The fixed panel was designed to map protein localization to five distinct subcellular regions of ciliated cells defined by the cilium (CL), the transition zone (TZ), the rootlet (RL), the cytoplasm, and the nucleus (Figure 2A). The selection of markers and antibodies was based on multiple criteria, including literature descriptions (e.g. UniProtKB), reliability of antibodies available in the HPA, IHC staining patterns in ciliated cells across the tissues of interest (Figure 2D), and compatibility with the mIHC workflow. The final panel was based on the following proteins: DNAH9 (Dynein Axonemal Heavy Chain 9), a component of the motile cilia axoneme(*19*); NPHP4 (Nephrocystin 4) localized in the TZ(*20–22*); CROCC (Rootletin), the main structural protein of the ciliary rootlet(*23*); AGR3 (Anterior Gradient Protein 3), described in mice as essential for regulating ciliary beat frequency(*24*); and the transcription factor FOXJ1 (Forkhead Box Protein J1), a key transcription factor for motile cilia formation(*16*, *25*) (Figure 2B; Supplementary Table 2). To validate the antibodies targeting the ciliary regions (CL, TZ, and RL), we performed confocal microscopy at 63X magnification (Figure 2C). Given the complex structure of the cilium, no substantial overlap was observed between these three markers, reinforcing confidence in the panel. This validation enabled the development of image analysis pipelines and the definition of regions of interests (ROIs) based on the signals obtained

from the fixed panel, corresponding to the five distinct subcellular localizations in ciliated cells (Supplementary Figure 1E).

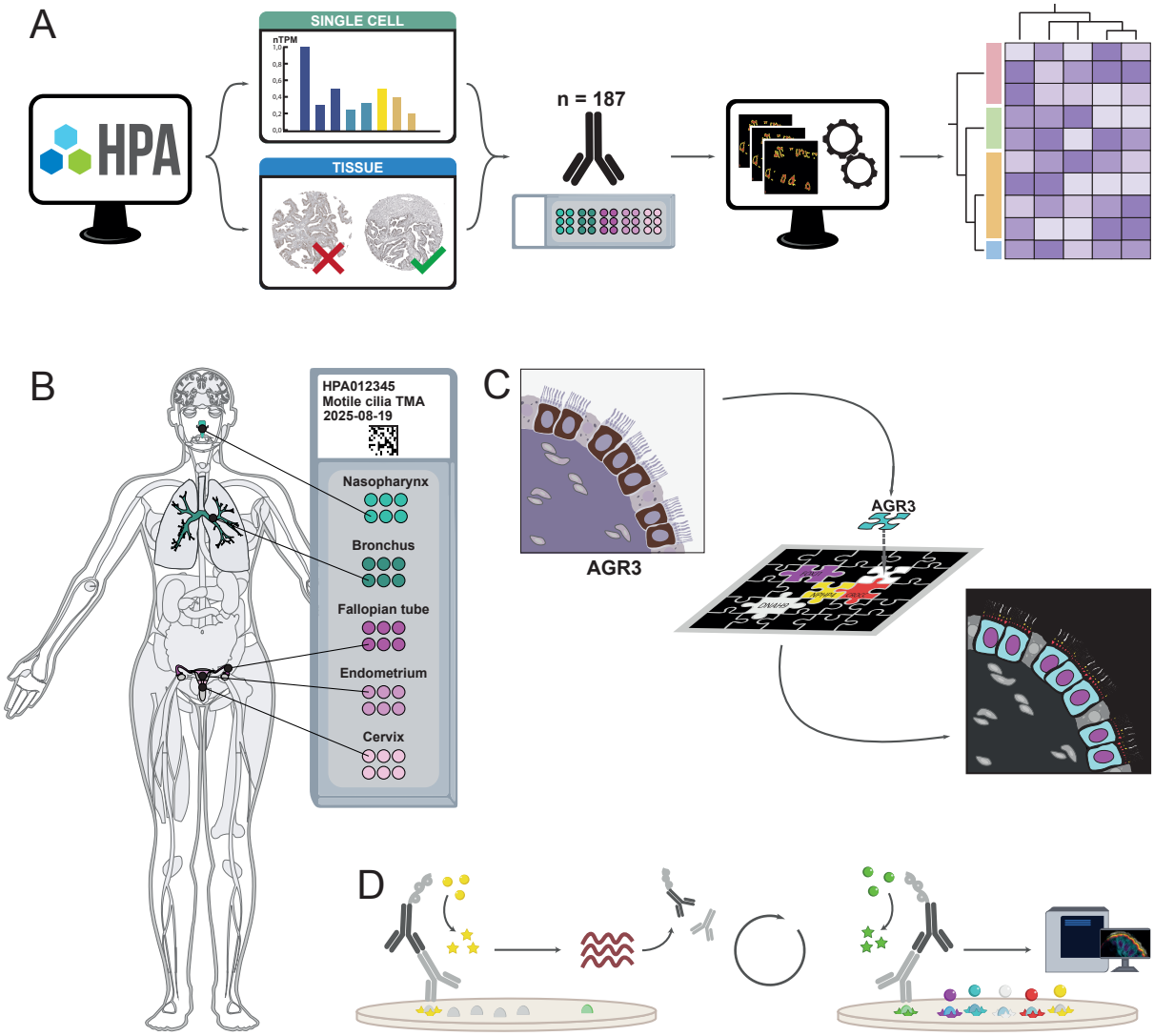


***Figure 1: Experimental design.*** **A)** Selection of protein candidates from the Human Protein Atlas (www.proteinatlas.org) using both the Single Cell and Tissue resources, allowing the identification of candidates expressed in ciliated cells with a reliable antibody (n=187). These candidates were stained alongside the fixed antibody panel. Each acquired image was automatically analyzed to

determine the expression profile, followed by clustering analysis. **B)** Five different tissues were collected and organized into a tissue microarray (TMA), consisting of two airway tissues (nasopharynx and bronchus) and three reproductive tissues (fallopian tube, endometrium, cervix). For each tissue, six cores from three patients were included. **C)** The fixed panel antibodies were selected based on a literature review and IHC staining comparisons available in the Tissue resource of the HPA, here exemplified by the protein AGR3, showing staining in the cytoplasm of ciliated cells. Antibodies with non-overlapping signals targeting different subcellular compartments of ciliated cells: nucleus (magenta), cytoplasm (cyan), rootlet (RL, red), transition zone (TZ, yellow), and cilium (CL, white) were combined into a multiplex immunohistochemistry (mIHC) panel. **D)** Schematic representation of the mIHC workflow, with the first and last cycles illustrated. The method relies on iterative cycles, each separated by heat-induced antibody stripping.

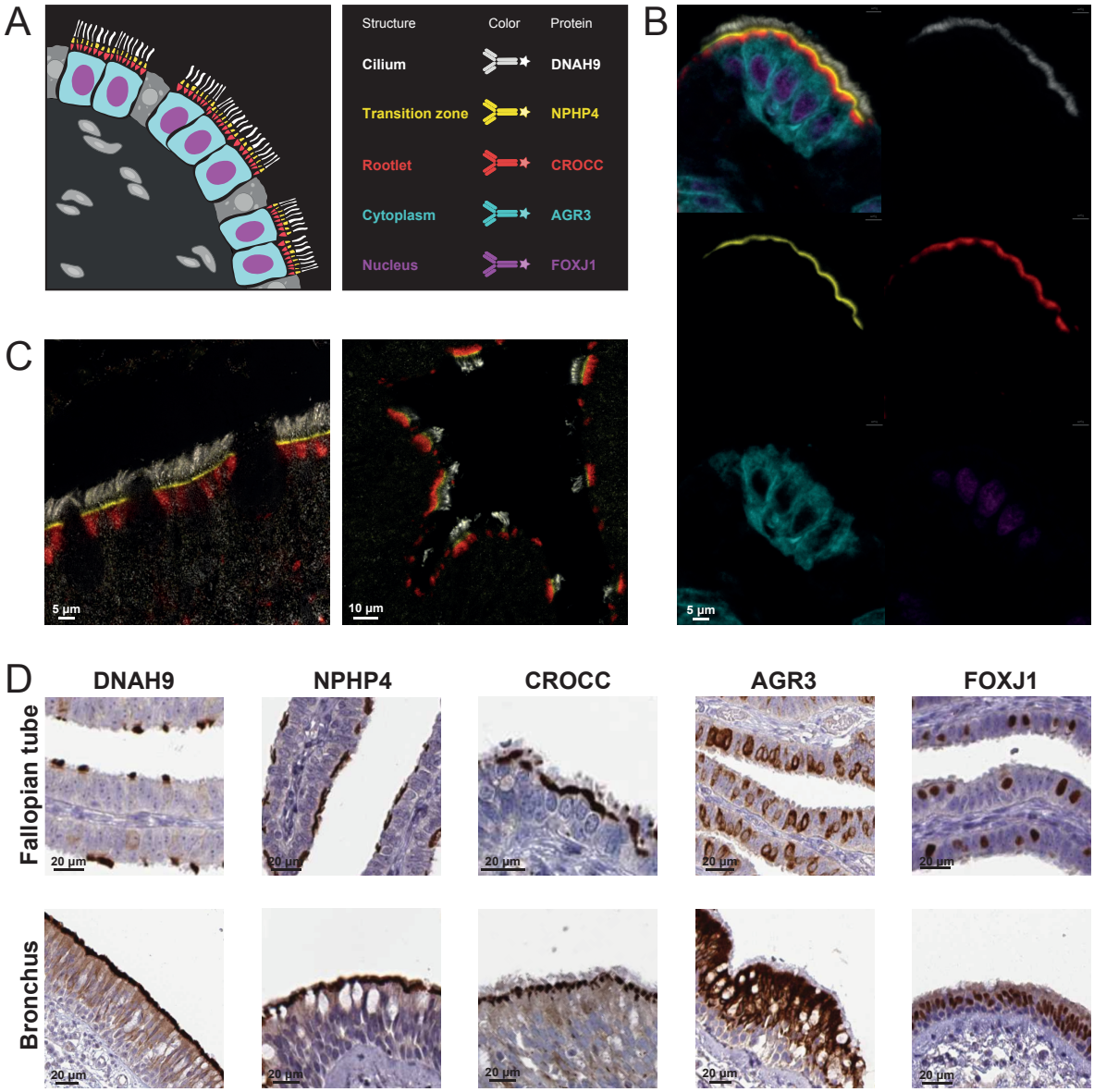


***Figure 2: Validation and characterization of the fixed antibody panel.*** **A)** Schematic overview of the fixed panel used for mIHC stainings. The mIHC panel included five antibodies targeting proteins expressed in specific subcellular structures of ciliated cells: DNAH9 for the cilium (CL, white), NPHP4 for the transition zone (TZ, yellow), CROCC for the rootlet (RL, red), AGR3 for the cytoplasm (cyan), and FOXJ1 for the nucleus (magenta). **B)** Staining of the 5-plex fixed panel in ciliated cells of the fallopian tube. Top left: all five antibodies combined; top right: CL; middle

left: TZ; middle right: RL; bottom left: cytoplasm; bottom right: nucleus. **C)** Confocal microscopy images. Confocal microscopy was used to validate the markers targeting ciliary structures. Non-overlapping signals representing the CL (white), TZ (yellow), and RL (red) are shown in the nasopharynx (left) and fallopian tube (right) at 63X resolution. **D)** IHC images from the HPA. Antibodies included in the panel were selected based on their staining patterns and reliability scores in the Tissue resource of the HPA.

***Subcellular mapping of protein expression in ciliated cells***

The selection of candidate proteins to be stained alongside the fixed panel was performed using both the Tissue and Single Cell resources of the HPA (Figure 1A). Candidate proteins were identified based on their normalized RNA expression levels in ciliated cell clusters from the Single Cell resource, prioritizing those with higher expression in ciliated cells compared to other cell types present in the studied tissues (Supplementary Figure 2). IHC staining patterns were examined across the five tissues, and antibody reliability was assessed based on the stringent criteria for determining specificity of antibodies in the Tissue resource of the HPA(*26*). A final list of 187 candidate proteins expected to be expressed in motile ciliated cells was compiled for staining with mIHC (Supplementary Table 3).

***Hierarchical clustering and functional annotation of ciliated cells proteins***

To address gaps in functional annotation, we integrated the FE scores defined by the HPP project(*26*) with our 187 protein candidates (Supplementary Table 4) to assess the functional

characterization of the proteins included in our study. Interestingly, just over a quarter (27%, n=51) of the candidate proteins stained alongside the panel fell into the FE1 category, indicating that at least one of their functions has been described. However, the majority (73%, n=136) remain poorly or partially characterized, with limited or no functional annotations (FE2 to FE5). To further examine the relationship between protein function and clustering, we analyzed the distribution of FE scores across clusters (Supplementary Figure 3). To provide a quantitative and systematic assessment of expression levels, we developed an automated image analysis workflow to quantify pixel intensity values for each analyzed protein and assess the subcellular localization of the staining patterns in relation to the fixed antibody panel (Supplementary Figure 1). To determine the overlap between each candidate protein and a specific area of the ciliated cells, the analysis method defined ROIs based on each panel marker individually. Pixel intensity values within these ROIs were then extracted from the images, allowing quantification of colocalization for each specific subcellular structure (Supplementary Figure 1). To account for multiple images per protein per ROI and per tissue, a median pixel intensity value was calculated per protein and tissue type for each ROI, generating an expression profile across the tissues. The resulting quantitative protein expression levels were subsequently used for hierarchical clustering, which identified seven distinct protein clusters (Figure 3B). Clustering was also performed on ROI per tissue type, revealing that CL and TZ regions consistently grouped together across all tissues. In contrast, RL, cytoplasm, and nucleus displayed more heterogeneous localization patterns, with the cytoplasm and RL exhibiting the highest variability across tissues. Gene ontology (GO) enrichment analysis was performed for each cluster across the three GO categories: biological process (BP), molecular function (MF) and cellular component (CC). This analysis aimed to validate the expression

patterns across different subcellular localizations and provide insights into the potential functions of the protein within each cluster (Figure 3C; Supplementary Table 5).

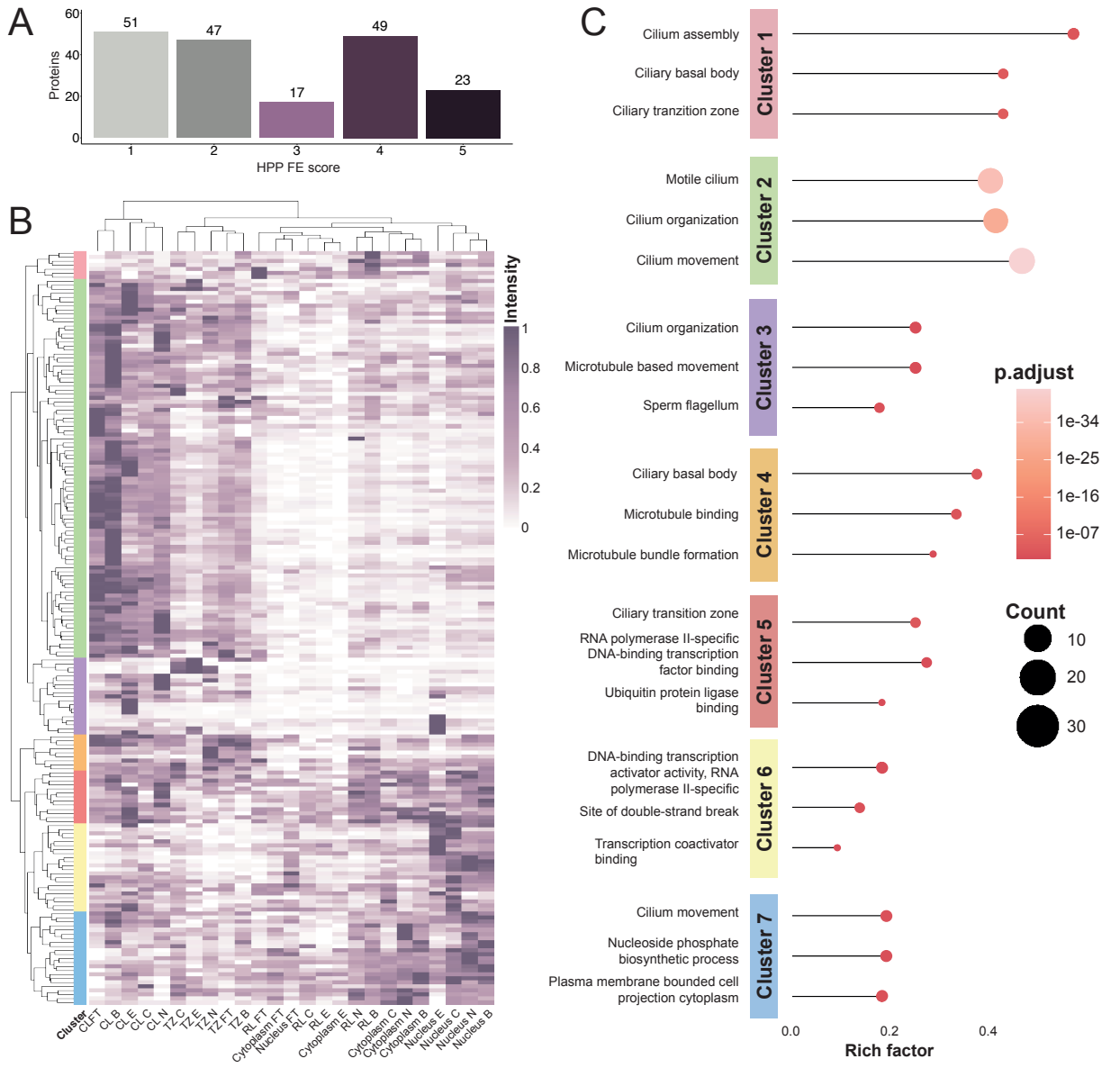


***Figure 3: Functional evidence, Clustering Analysis, and Gene Ontology Enrichment.*** **A)** Bar plot showing the distribution of the studied protein between the different FE scores (FE1-5). **B)** A heatmap was generated based on expression levels obtained from image analysis for each

candidate protein across different subcellular localizations and tissues (Fallopian tube (FT), Bronchus (B), Endometrium (E), Cervix (C), and Nasopharynx (N). Hierarchical clustering was applied to both rows and columns. The columns were primarily clustered according to subcellular localization rather than tissue type, particularly for ciliary structures such as the cilium (CL) and transition zone (TZ). Row clustering identified seven distinct clusters based on the expression patterns of the 187 candidate proteins. **B)** Bubble plot showing the top three Gene Ontology (GO) terms of the three categories (BP, MF and CC) per cluster, with enrichment levels represented by the rich factor i.e. the proportion of input genes annotated to a specific term relative to the total genes associated with that term.

*Cluster 1: Basal body and ciliary core*

Cluster 1 (n = 7, primarily expressed in the RL, Figure 3B), was strongly linked to cilia, as indicated by its top GO terms: cilium assembly, ciliary basal body, and ciliary transition zone (Figure 3C). This suggests that proteins in this cluster play a central role in ciliary function. One notable example is MDM2, which localized to the RL of the cilia in all five tissues and showed a strong concordance between image observation and image analysis results (Figure 4A). Interestingly, none of the 65 GO terms associated with MDM2 in our analysis; including response to magnesium ion, cellular response to estrogen stimulus, positive regulation of intracellular protein transport, and negative regulation of cell cycle G1/S phase transition; are directly related to cilia or their structure. Although MDM2 is an FE1 protein with at least one well-characterized function, its role in ciliated cells remains unclear.

*Cluster 2: Axonemal and motile cilia proteins*

Cluster 2 harbored the largest number of proteins (n = 94), with the top GO terms: motile cilium, cilium organization, and cilium movement, indicating a strong association with motile cilia specifically, rather than cilia in general (Figure 3C). The proteins in this cluster were primarily detected in CL across all five analyzed tissues (Figure 3B). One example is NME9 (NME/NM23 family member 9, also known as TXNDC6 or TXL-2) (Figure 4B). While NME9 is highly expressed in multiple tissues, with the highest mRNA level detected in the testis, previous studies have shown that it localizes to airway epithelial cilia as a microtubule binding protein(*27*). Here, we demonstrated that NME9 is not restricted to the airway epithelium but is also present in the motile cilia of three female reproductive tissues, where it exhibited similar staining intensity. Another protein in Cluster 2 is LRRC73 (Leucine rich repeat containing 73) (Figure 4B). The mIHC analysis indicated that LRRC73 was equally expressed in CL and RL but absent in TZ, with a consistent pattern across all five tissues. However, no GO terms were identified for LRRC73 in our analysis, nor are functional annotations available in UniProt, and it is ranked as a FE5 protein (Supplementary Table 4 and 5). A third example is DPCD (Deleted in primary ciliary dyskinesia homolog) (Figure 4B), a protein implicated in the function or formation of ciliated cells. Its highest gene expression was observed in the testis, and previous studies have shown it is expressed in sperm(*28*). Our analysis confirmed that DPCD was specifically detected in CL of motile cilia in all five tissues, with stronger expression in airway epithelial cilia compared to those in the female reproductive tract. In humans, DPCD interacts with RUVBL1 and RUVBL2, proteins known to be crucial for the initiation of ciliogenesis of primary cilia(*29–31*). RUVBL1, which fell into Cluster 7, was detected in the cytoplasm and nucleus of ciliated cells but not in the ciliary structure

(Figure 5C), in line with previous findings. GO terms identified for RUVBL1 include dynein axonemal particle, TFIID-class transcription factor complex binding, and ADP binding (Supplementary Table 4). Notably, *Ruvbl1* knockdown in mice leads to axoneme structural defects, further supporting its role as a ciliopathy-related protein essential for ciliary integrity(*31*). Another protein found to be in Cluster 2 was ARMC2 (FE2), located in the cilium across all five tissues (Supplementary Figure 4). It has been shown that PCD caused by *ARMC2* mutations not only affects the reproductive system and abnormalities in sperm flagella (*32*), but also results in an impaired airway system (*33*). Here, spatial evidence is provided showing ARMC2 to be present in motile cilia in both female reproductive and airway epithelium (Supplementary Figure 4). Our analysis connected ARMC2 to multiple GO terms, such as cilium organization, cilium assembly, and spermatid development. Finally, KIAA2012, a poorly characterized protein with no known function (FE5) (Figure 4B; Supplementary Table 5) was also found in this cluster. Our data revealed that it localized to CL of motile cilia across all five tissues, with similar expression levels throughout, suggesting a conserved ciliary function.

*Cluster 3: Ciliary and flagellar motility proteins*

The top GO terms for Cluster 3 (n= 19), were cilium organization, microtubule-based movement, and sperm flagellum (Figure 3C), highlighting its association with ciliary and flagellar structures. One notable protein in this cluster is MS4A8 (Membrane spanning 4-domains A8, also known as MS4A8b) (Figure 4C), a member of the MS4A protein family, that shares sequence and structural homology with the IgE receptor CD20(***34***). Here, we demonstrated that MS4A8 is specifically localized to CL of motile ciliated cells across all five tissue types. MS4A8 has been ranked FE4

and interestingly also lacks previous evidence at the protein level (Supplementary Table 5). Our findings here provide spatial evidence of MS4A8 protein expression, offering a valuable insight into its potential role in motile cilia function.

*Cluster 4: Dual localization in axoneme and transition zone*

Cluster 4 (n = 9, with no FE1 proteins, Supplementary 3), presented a more complex expression pattern, with overrepresentation in both CL and TZ (Figure 3B). The top GO terms identified were ciliary basal body, microtubule binding, and microtubule bundle formation (Figure 3C), highlighting the potential structural roles of these proteins in cilia. One key protein in this cluster was SPAG6 (Sperm associated antigen 6) (Figure 4D), which is strongly linked to microtubule bundle formation, cilium organization, and cilium movement (Supplementary Table 5). SPAG6 is crucial for maintaining normal ciliary structure and function, and its loss has been associated with brain edema in mice(*35*, *36*). While SPAG6 deficiency leads to male infertility, female mice remain fertile, although fertilization is delayed, suggesting an impact on the motile cilia in the oviduct(*37*). In this study, SPAG6 showed widespread expression across the whole cell in bronchus and nasopharynx, while its localization was more restricted to CL and TZ in endometrium and cervix (Figure 4D). Another protein in this cluster is LRRC45 (Leucine rich repeat containing 45), which was primarily localized to CL, as well as TZ and RL (Figure 4D). Previously described in primary cilia, defects of LRRC45 are thought to alter ciliary length and beat frequency(*38*, *39*). Here, we showed its presence and specific localization in motile cilia across both the respiratory and reproductive tract. However, our GO term analysis did not identify

any functional annotation for LRRC45, and it is classified as FE5 (Supplementary Table 5), indicating that its precise role remains to be elucidated.

*Cluster 5: Ciliated proteins with diverse localization*

In Cluster 5 (n = 13), protein expression patterns were distributed across the entire ciliated cell (Figure 3B). The GO terms identified in this cluster were ciliary transition zone, RNA polymerase II-specific DNA-binding transcription factor binding, and Ubiquitin protein ligase binding, suggesting a broad functional involvement in cellular activity (Figure 3C). One example is RIIAD1 (Regulatory subunit of type II PKA R-subunit domain containing 1), which was predominantly localized in CL, TZ, cytoplasm and nucleus across all examined tissues (Figure 5A). Although RIIAD1 remains poorly characterized, studies have reported its upregulation in breast cancer tumors(*40*, *41*). Notably, our GO term analysis did not identify any functional annotations for this protein, which is classified as a FE5 protein (Supplementary Table 4), suggesting its role in motile cilia should be examined. Another protein in this cluster is SGMS2 (Sphingomyelin synthase 2), which was detected in all targeted locations in the ciliated cells across all tissues, although significantly lower presence was observed in RL in the reproductive tissues (Figure 5A). SGMS2 is classified as a FE1 protein (Supplementary Table 4), indicating strong evidence for a molecular function. While our GO term analysis identified phosphotransferase activity for other substituted phosphate groups as a related term (Supplementary Table 5), additional annotations, including nucleoplasm, plasma membrane, and sphingomyelin synthase activity, suggest broader functional roles.

*Cluster 6: Nuclear and cytoplasmic proteins*

Cluster 6 (n = 22) consisted of proteins primarily localized to the cytoplasm and nucleus (Figure 3B), as supported by the top three GO terms: DNA-binding transcription activator activity, RNA polymerase II-specific, site of double-strand break, and transcription coactivator binding (Figure 3C). Notably, 45% of the proteins (n=10) in this cluster are classified as FE1, indicating strong evidence of the molecular function (Supplementary Figure 3). One key protein of this cluster is WRAP53 (WD repeat containing antisense to TP53) (Figure 5B), classified as FE1 (Supplementary Table 4). The GO term enrichment identified the site of double-strand break as a related function (Supplementary Table 5), aligning with its known role in DNA damage response. WRAP53 is recruited to the site of a double strand break (DSB), where it facilitates the recruitment of other DNA repair proteins(*42*). Here, we showed that WRAP53 was predominantly expressed in the nucleus of ciliated cells across all tissues. Another protein in this cluster is SAMHD1 (SAM and HD domain containing deoxynucleoside triphosphate triphosphohydrolase 1) (Figure 5B), also classified as FE1 (Supplementary Table 4). Like WRAP53, SAMHD1 is associated with the GO term site of double-strand break (Supplementary Table 4). We revealed its nuclear localization in ciliated cells across all five tissues, reinforcing its potential role in DNA repair mechanisms.

*Cluster 7: mixed localization with ciliary and cytoplasmic functions*

The final cluster, Cluster 7 (n = 23), exhibited less specific localization patterns compared to other clusters, with proteins predominantly found in the cytoplasm and the nucleus (Figure 3B). GO term analysis identified key biological functions, including cilium movement, nucleoside

phosphate biosynthetic process, and plasma membrane bounded cell projection cytoplasm (Figure 3C). Among the proteins in this cluster, RUVBL1 was previously mentioned with proteins from cluster 2 (Figure 5C) and classified as FE1 (Supplementary Table 4). Another protein in this cluster is CFAP73 (Cilia and flagella associated protein 73), classified as FE4 (Supplementary Table 4), which was primarily expressed in the cytoplasm and, to a lesser extent, in the nucleus across all tissues (Figure 5C). GO analysis linked CFAP73 to essential ciliary processes, including cilium movement, axonemal dynein complex assembly, and cilium organization (Supplementary Table 5), suggesting a role in ciliary structure and function.

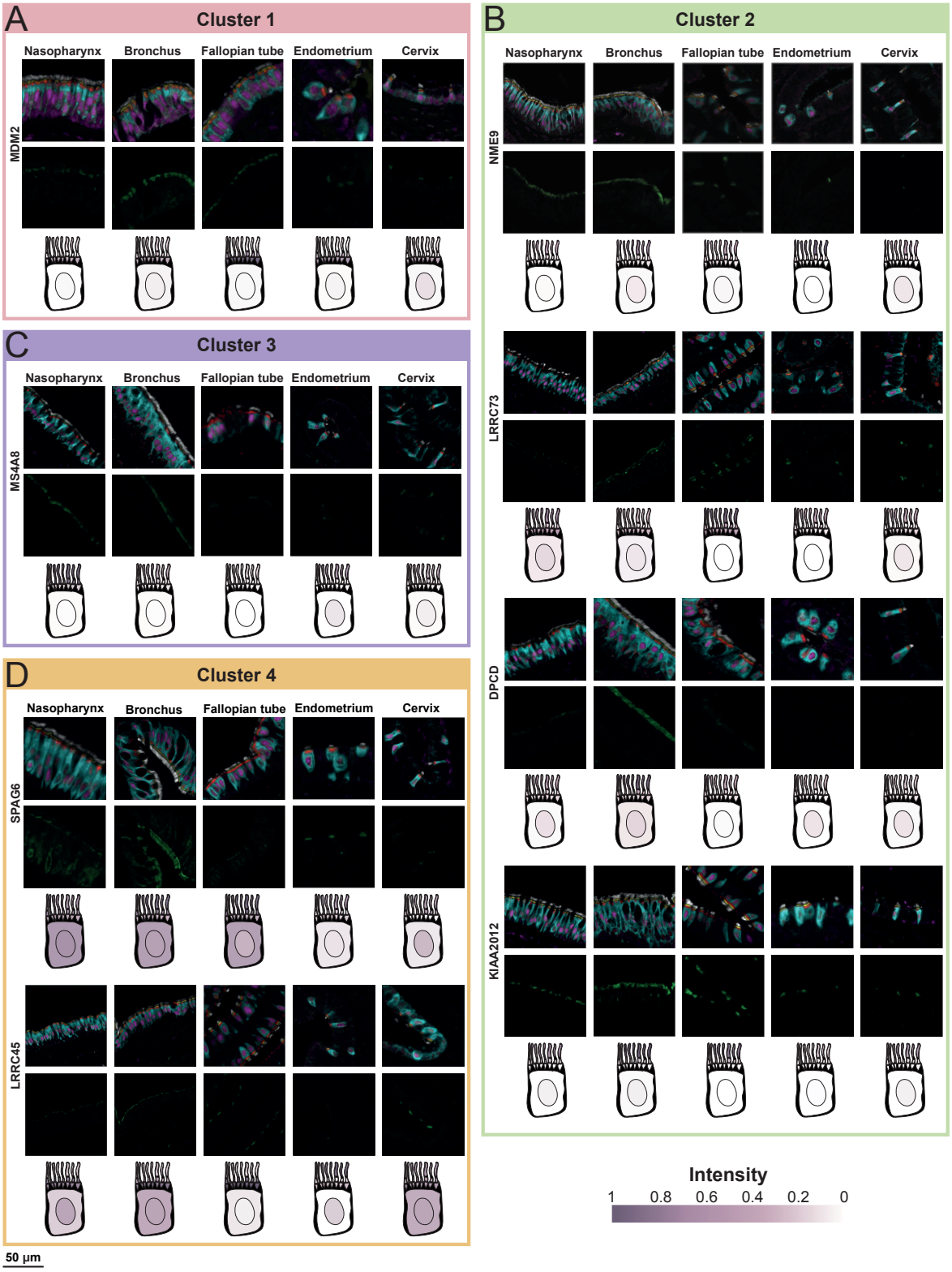


***Figure 4: mIHC staining of representative proteins from each cluster across different tissues.***

The top row of images shows the composite staining, including the fixed panel and the candidate

protein. The bottom row displays only the candidate protein (in green). Below the images, a schematic representation of a ciliated cell illustrates the expression levels obtained from image analysis for each subcellular localization. A) Cluster 1: MDM2 (RL) B) Cluster 2: NME9 (CL), LRRC73 (CL and RL), DPCD (CL), and KIAA2012 (CL). C) Cluster 3: MS4A8 (CL). D) Cluster 4: SPAG6 (whole cell in bronchus and nasopharynx; CL and TZ in endometrium and cervix) and LRRC45 (CL, TZ and RL).

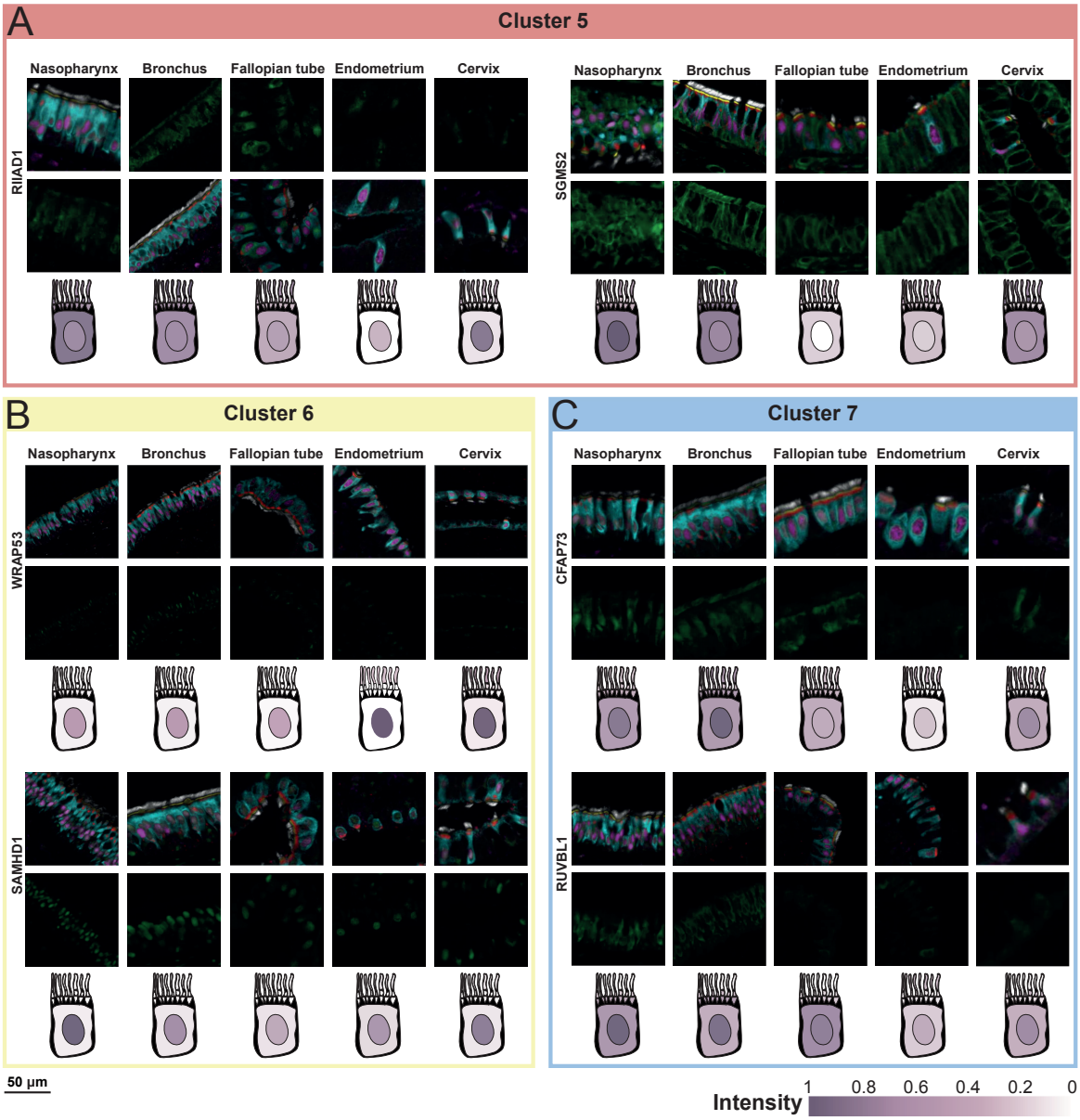


***Figure 5: mIHC staining of representative proteins from each cluster across different tissues.*** The top row of images shows the composite staining, including the fixed panel and the candidate protein. The bottom row displays only the candidate protein (in green). Below the images, a schematic representation of a ciliated cell illustrates the expression levels obtained from image analysis, the darker the color, the higher the expression level. **A**) Cluster 5: RIIAD1 (CL, TZ,

cytoplasm and nucleus) and SGMS2 (whole cell). **B**) Cluster 6: WRAP53 (nucleus) and SAMHD1 (nucleus). **C**) Cluster 7: CFAP73 (cytoplasm and nucleus) and RUBBL1 (cytoplasm and nucleus).

## Discussion

This study introduces a comprehensive mIHC and automated image analysis workflow designed to investigate the subcellular localization of proteins in motile ciliated cells at a high resolution. To our knowledge, this is the first approach to combine high-resolution tissue imaging of motile ciliated cells with the scalability of high-throughput analysis of a large set of proteins across multiple tissue types using an in-house medium-plex panel tailored for this purpose. The unique panel and novel workflow were successfully used to spatially map 187 proteins in ciliated cells across five human tissues from both respiratory and female reproductive tracts. Protein localization was determined based on the overlap with a fixed reference panel outlining distinct subcellular compartments of motile ciliated cells. The validated panel enabled precise localization and quantification of each of the candidate proteins within five defined subcellular regions: the nucleus, cytoplasm, and three cilia-specific compartments: CL, TZ, and RL(*17*).

The 187 candidate proteins studied in the present investigation were selected using two key resources of the Human Protein Atlas (HPA): i) the Single Cell resource, to validate the transcript-level expression in ciliated cells compared to other cell types in the studied tissues, and ii) the Tissue resource, to prioritize candidates with reliable antibodies showing positive IHC staining in ciliated cells in at least one of the five analyzed tissues included in the study. This selection process enabled us to study not only well-characterized proteins in cilia (such as CCDC39(*43*, *44*), and

DNAH7(*45*, *46*)) but also a set of proteins with no previous description in ciliated cells (such as KIAA2012).

While most of the proteins encoded by the human genome have been credibly identified, many proteins still lack a specifically defined function based on experimental evidence. One of the major goals of the international consortium HPP is to gain a solid understanding of at least one function for every protein at the molecular level(*47*). As a result, the HPP has introduced the definition of Function Evidence (FE) scores that build upon the functional information available in the UniProtKB, described as FE1-FE5 according to the level of evidence for a molecular function(*48*). These new FE scores have been implemented for each protein encoded by the human genome. Interestingly, a majority (73%) of the candidate proteins characterized in our study showed FE2-FE5 scores, indicating that a full understanding of the role of these proteins in ciliated cells is still lacking. Our stringent validation pipeline and detailed data presenting a specific localization to ciliated cells at a subcellular resolution gives further insights into a presumed function of these proteins. The spatial localization data constitutes a starting point for further functional studies using e.g. model systems, to determine the roles of these proteins in each of the analyzed tissue types.

For further functional analysis, we also performed a hierarchical clustering analysis of the candidate proteins for each of the analyzed tissues using quantitative protein localization data generated by automated image analysis. The clustering analysis revealed that protein localization was largely conserved across tissues, particularly for CL and TZ, suggesting a shared spatial distribution for these proteins. Similarly, candidate proteins clustered based on their expression patterns, resulting in seven distinct expression groups. While some clusters exhibited clear localization patterns, such as cluster 2, with proteins mainly expressed in the cilium, or cluster 6,

in the nucleus; others, like cluster 5, displayed a more dispersed expression profile. Nevertheless, the clustering analysis allowed us to group the proteins according to expression patterns, highlighting numerous poorly described proteins that shared a similar expression profile with well-described cilia markers, thus indicating a similar molecular function. We also performed a GO analysis for each of the expression clusters, indicating a clear overrepresentation of ciliary functions, thus validating our strategy.

In the present investigation, we shed light on the detailed subcellular localization of proteins expressed in motile ciliated cells for several proteins not previously described in the context of cilia biology. One example is KIAA2012, a poorly described protein located in the cilium (CL region) of motile cilia in both respiratory and female reproductive tissues. Based on its subcellular location, it can be anticipated that this protein may contribute to cilia motility and thereby has the potential to cause primary ciliary dyskinesia (PCD) where the function of motile cilia is impaired, a syndrome causing a wide range of symptoms and diseases(*11*). Another not well studied protein is RIIAD1, previously shown to be upregulated in breast cancer tumors, but without a known molecular function. The name of the protein suggests that it regulates a subunit of protein kinase A (PKA), involved in endocrine signaling and previously described to play a crucial role in regulating ciliary beating frequency(*49*). Here, we show that this protein is generally expressed across the whole ciliated cell, both in the cell body and the cilium, in all five analyzed tissues. Interestingly, scRNA levels in other analyzed tissues in the Single Cell resource of the HPA show that expression is dominated in ciliated cells, followed by early spermatids, and cone photoreceptor cells. As mature sperm contain flagella, with a similar molecular function related to motility as ciliated cells(*50*), and photoreceptor cells contain specialized sensory cilia(*51*), the mRNA expression levels together with the spatial localization pattern suggests that this protein may be

crucial for regulating and supporting key ciliary functions. In addition to KIAA2012 and RIIAD1, our study included numerous other proteins that lack a description of molecular function or were not previously described in the context of cilia biology, including MS4A8 which previously only has been described at the transcript level. Here, we could provide the first spatial evidence that this protein is expressed in the cilium of motile ciliated cells.

The selection of proteins included in the present investigation was mostly focusing on conserved motile ciliary proteins present in all the analyzed tissues, but we did identify several proteins whose expression pattern differed between respiratory and reproductive tissues. This shows that our workflow has the potential of cross-tissue comparison and that motile cilia may have different proteomes in different human tissue compartments, a finding that may explain phenotypic diversity in motile ciliopathy patients. Further studies using our novel strategy for mapping the entire motile cilia proteome in health and disease are expected to give unprecedented insights into the field of cilia biology.

Importantly, our method is facing limitations in resolution: Proteins detected in the TZ region might not necessarily be part of the TZ but localize close to it, at the rootlet or at the proximal cilium. Similarly, proteins that we discover in the CL region might not localize in the axoneme but in the cilioplasm or ciliary membrane. And we might detect proteins in the RL region that belong either to the RL or to broader structures close to the RL or in the basal body (BB).

In the rapidly expanding field of spatial biology, a multitude of methods focus on multiplexed imaging of proteins. Here, we developed a novel “medium-plex” workflow, centered around a fixed antibody panel outlining five different subcellular compartments of motile ciliated cells. While higher-plex methods enable the simultaneous analysis of multiple cell types and structures

within a given tissue, our approach offers the advantage of subcellular-level resolution combined with high-throughput capacity, making it well suited for both proteome-wide investigation and clinical routine. This strategy provides a powerful foundation for comprehensive mapping of the motile cilia proteome in both health and disease. It represents an important step toward uncovering the molecular mechanisms driving ciliopathy and paves the way for future applications in precision diagnostics and personalized medicine.

## Materials and Methods

### *Ethics and tissue microarray design*

Human tissue samples from five tissue types were obtained from Uppsala University Hospital, Sweden, and collected within the Uppsala Biobank organization. All samples were anonymized in accordance with the approval and advisory report of the Uppsala Ethical Review Board (ref nos. 2002-577, 2005-388, 2007-159). The tissue microarray (TMA) was generated as previously described(*52*) and comprised five distinct tissues: fallopian tube, endometrium, cervix, nasopharynx, and bronchus (Figure 1B). Each tissue was represented by six one mm diameter cores, with duplicate cores from three individuals. Patient information is provided in Supplementary Table 1. The TMA was sectioned into 4 µm sections using a waterfall microtome (Microm H355S, ThermoFisher Scientific, Fremont, CA) and mounted onto SuperFrost Plus slides (Thermo Fisher Scientific, Fremont, CA). The slides were dried at room temperature (RT) overnight, baked at 50°C for 12–24 hours, cooled, and stored at RT until further use.

***Panel development and candidate selection***

A 6-plex panel was built to target five regions in ciliated cells: the cilium (CL), transition zone (TZ), rootlet (RL), cytoplasm, and nucleus. Protein markers and corresponding antibodies have been selected based on i) literature search (e.g. UniProtKB), ii) antibody IHC validation score on HPA, iii) IHC staining patterns in ciliated cells in nasopharynx, bronchus, fallopian tube (FT), endometrium, and cervix, and iv) compatibility in the multiplex immunohistochemistry (mIHC) panel and workflow. Each antibody was first tested with a single-plex run to ensure that it works with the OPAL detection system. Then, each antibody was tested in each position of the 6-plex, except the third location reserved for the candidate protein, to find the best location for each antibody and ensure a trustable staining pattern and a stable panel (Supplementary Table 2). To validate the three markers targeting the cilium, confocal microscopy at 63X was conducted using Leica STELLARIS 5 (Leica Microsystems, Illinois, US).

***Slide pretreatment***

To remove paraffin and rehydrate tissue cores, a ST5010 Autostainer XL (Leica Biosystems, Baden-Württemberg, Germany) was used with the following protocol: Xylene (5 min), Xylene (5 min), Xylene (1 min), absolute ethanol (3 min), absolute ethanol (3 min), 96% ethanol (3 min), 96% ethanol + 0.3% $H_2O_2$ (5 min), 80% ethanol (3 min), and $dH_2O$ (30 sec). The slides were then stored in deionized water until antigen retrieval.

Antigen retrieval was performed to expose protein epitopes for antibody binding. Slides were subjected to heat-induced epitope retrieval (HIER) in pH 6 buffer (Agilent Technologies Inc., Santa Clara, CA, USA) at 125°C for 4 min using a Biocare Medical Decloaking Chamber™ PLUS (DC2008INTL). After cooling to 90°C, the slides were rinsed in deionized water (1–2 min) and transferred to TBS-Tween wash buffer (Thermo Fisher Scientific, TA-999-TT, Waltham, MA, USA) until further processing. To reduce autofluorescence, slides were incubated in a bleaching buffer containing 1.5% hydrogen peroxide, 0.2 M glycine, and 1X TBS-Tween (Thermo Fisher Scientific, TA-999-TT) in 50-mL Falcon tubes. Tubes were rotated in LED light at RT for 1 hour using a Stuart SRT9D roller mixer. Slides were subsequently washed and stored in TBS-Tween until further use.

***Multiplex immunofluorescence***

For multiplex immunofluorescence (mIF) staining, one slide per candidate protein was used. Each staining cycle proceeded as follows: Tissue sections were blocked with UV Blocking Buffer (10 min), incubated with primary antibody (30 min), rinsed in TBS-Tween, incubated with HRP-conjugated secondary antibody (10 min), and washed again in TBS-Tween. Slides were then incubated with the cycle-specific OPAL™ fluorophore (Akoya Biosciences) for 10 min, rinsed, and subjected to HIER (90°C, pH 6 buffer, 20 min). The order of the Opals and panel markers from first to last cycle was: OPAL690 for CROCC, OPAL620 for DNAH9, OPAL520 for candidate protein (changed for each slide), OPAL570 for AGR3, OPAL480 for NPHP4, and OPAL-DIG-780 for FOXJ1. After each cycle, slides were rinsed and stored in wash buffer. The final step involved incubating slides with OPAL 780 fluorophore-conjugated anti-DIG antibody

(1:125 in Antibody Diluent) for 1 hour, followed by staining with DAPI (1:1000, Invitrogen, D1306, Thermo Fisher Scientific) for 5 min. Slides were rinsed, mounted with Invitrogen ProLong™ Glass Antifade Mountant, covered, and cured overnight. Finally, slides were digitized at 40X magnification using PhenoImager (Akoya Biosciences).

***Image analysis***

A manual quality control was performed on all tissue cores, ensuring representativity of the staining pattern, presence of ciliated cells and normal tissue histology. Tissue cores that did not pass this quality control were not included in the data analysis. Automated image analysis was conducted in ImageJ Fiji(*53*) to generate quantitative data. TIFF image stacks were processed per TMA core (Supplementary Figure 1A). Each stack contained separate images for panel marker proteins, DAPI, and autofluorescence. Images were converted to 8-bit, and DAPI/autofluorescence images were discarded (Supplementary Figure 1B). Segmentation was performed using 3-level Multi Otsu thresholding(*54*), where only the highest threshold level (brightest pixels) was used (Supplementary Figure 1C). If segmentation failed for any marker, the stack was excluded from further analysis. For each panel marker image, segmentation masks were generated (Supplementary Figure 1D), defining regions of interest (ROIs) corresponding to each marker and candidate protein (Supplementary Figure 1E). ROIs were used to extract pixel values from candidate protein images by measuring the pixel value within each ROI, including mean pixel intensity, maximum intensity, minimum intensity, and total ROI area per core.

***Data analysis***

Data analysis was performed using R 4.4.2. Median intensity values were calculated per ROI (CL, TZ, RL, cytoplasm, nucleus) for each protein and tissue, identifying predominant colocalization patterns. Cores excluded during manual annotation were omitted from median calculations. Data were normalized via Min-Max scaling per protein and slide across all tissues, with values rescaled between 0 and 1. Heatmaps were generated using the pheatmap package (v1.0.12). Gene Ontology (GO) enrichment analysis was conducted using clusterProfiler (v4.14.6) and the human gene reference database org.Hs.eg.db (v3.20.0), retrieved on 2025-02-25. Only GO terms with $p < 0.05$ were retained. The top three terms per cluster were selected based on the highest number of associated proteins. The Protein Evidence (PE) and Function Evidence (FE) scores for the candidate proteins were downloaded from the HPP portal (*55*) on 2025/02/13.

ASSOCIATED CONTENT

The following files are available free of charge (separate file (s)).

**Supplementary Figure 1:** Image analysis workflow

**Supplementary Figure 2:** mRNA expression levels across different cell types based on scRNA sequencing data for the 187 candidates included in the study

**Supplementary Figure 3.** Bar plot showing the distribution of FE scores across each expression **cluster.**

**Supplementary Figure 4.** mIHC staining of ARMC2 in the cilium in different tissues.

**Supplementary Table 1:** Patient information for all tissue samples included in the TMA

**Supplementary Table 2:** Information for the antibodies included in the fixed panel

**Other Supplementary Materials for this manuscript include the following:**

**Supplementary Table 3:** Information for the antibodies corresponding to the 187 protein candidates included in the study (separate .xlsx file)

**Supplementary Table 4:** Protein Evidence (PE) and Function Evidence (FE) scores from the HPP for the 187 candidate proteins included in the study (separate .xlsx file)

**Supplementary Table 5:** Protein expression levels based on automated image analysis, and results based on gene ontology enrichment for the 187 protein candidates included in the study (separate .xlsx file)

AUTHOR INFORMATION

Corresponding author:

Cecilia Lindskog

Department of Immunology, Genetics and Pathology

Cancer Precision Medicine Research Unit

Uppsala University, SE-75185 Uppsala, Sweden

Tel: +46 18 471 50 32

Email: cecilia.lindskog@igp.uu.se

Author Contributions

Conceptualization: CL and LM; Data curation: FB and LM; Formal Analysis: FB and LM; Funding acquisition: CL and MU; Investigation: FH, LM, JNH, FB; Methodology: CL, FB, LM and FH; Project administration: CL and LM; Resources: CL and LM; Image analysis: FB, FH, LM; Supervision: CL, LM, FH; Validation: FB, LM, and CL; Visualization: FB and LM; Writing – original draft: FB, LM and CL; Writing – review & editing: FB, LM, CL, FH, JNH and MU. All authors have read and approved the final version of the manuscript.

Funding Sources

CL: Swedish Research Council (2022–02742)

MU: Knut and Alice Wallenberg Foundation (2015.0344)

JNH: Postdoctoral Fellowship from the Wenner-Gren Foundations and by an EMBO Postdoctoral Fellowship (ALTF 556-2022)

Notes

Competing interests: Authors declare that they have no competing interests.

***Data availability***

Out of the 187 proteins, 149 were made available on the atlas in for the latest version (v25). The remaining will be available for the next update of HPA during 2025.

***Code availability***

The script for image analysis (Macros) and data analysis (R) used for data analysis and visualization will be available on GitHub at time of submission:

github.com/LindskogLab/Subcellular-map-of-proteins-in-ciliated-cells

ACKNOWLEDGMENT

We thank the Biological Visualization platform BioVis at Uppsala university for their vast help in ´imaging and image analysis. We also thank the patients who donated tissues for HPA. Lastly, we thank the members of HPA supporting this project in any way, especially Jonas Gustavsson, Rutger Schutten, and Borbala Katona.

ABBREVIATIONS

AI - artificial intelligence; B – bronchus; BB – basal body; BP - biological process; C - cervix; CC - cellular component; CL - cilium; DSB - double-strand break; E - endometrium; FE - function evidence; FT - fallopian tube; GO - gene ontology; HIER - heat-induced epitope retrieval; HPA - Human Protein Atlas; HPP - Human Proteome Project; HRP - horseradish peroxidase; IgE – immunoglobulin E; IHC - immunohistochemistry; MF - molecular function; mIHC - multiplex immunohistochemistry; N - nasopharynx; PCD - primary ciliary dyskinesia; PE - protein evidence; PKA – protein kinase A; QC - quality control; RL - rootlet; ROI - regions of interest; RT - room temperature; scRNA - single-cell RNA; TMA - tissue microarray; TZ - transition zone

REFERENCES

1. M.-C. Hung, W. Link, Protein localization in disease and therapy. *J. Cell Sci.* **124**, 3381–3392 (2011).

2. P. J. Thul, L. Åkesson, M. Wiking, D. Mahdessian, A. Geladaki, H. Ait Blal, T. Alm, A. Asplund, L. Björk, L. M. Breckels, A. Bäckström, F. Danielsson, L. Fagerberg, J. Fall, L. Gatto, C. Gnann, S. Hober, M. Hjelmare, F. Johansson, S. Lee, C. Lindskog, J. Mulder, C. M. Mulvey, P. Nilsson, P. Oksvold, J. Rockberg, R. Schutten, J. M. Schwenk, Å. Sivertsson, E. Sjöstedt, M. Skogs, C. Stadler, D. P. Sullivan, H. Tegel, C. Winsnes, C. Zhang, M. Zwahlen, A. Mardinoglu, F. Pontén, K. von Feilitzen, K. S. Lilley, M. Uhlén, E. Lundberg, A subcellular map of the human proteome. *Science* **356**, eaal3321 (2017).

3. S. Adhikari, E. C. Nice, E. W. Deutsch, L. Lane, G. S. Omenn, S. R. Pennington, Y.-K. Paik, C. M. Overall, F. J. Corrales, I. M. Cristea, J. E. Van Eyk, M. Uhlén, C. Lindskog, D. W. Chan, A. Bairoch, J. C. Waddington, J. L. Justice, J. LaBaer, H. Rodriguez, F. He, M. Kostrzewa, P. Ping, R. L. Gundry, P. Stewart, S. Srivastava, S. Srivastava, F. C. S. Nogueira, G. B. Domont, Y. Vandenbrouck, M. P. Y. Lam, S. Wennersten, J. A. Vizcaino, M. Wilkins, J. M. Schwenk, E. Lundberg, N. Bandeira, G. Marko-Varga, S. T. Weintraub, C. Pineau, U. Kusebauch, R. L. Moritz, S. B. Ahn, M. Palmblad, M. P. Snyder, R. Aebersold, M. S. Baker, A high-stringency blueprint of the human proteome. *Nat. Commun.* **11**, 5301 (2020).

4. M. Uhlén, L. Fagerberg, B. M. Hallström, C. Lindskog, P. Oksvold, A. Mardinoglu, Å. Sivertsson, C. Kampf, E. Sjöstedt, A. Asplund, I. Olsson, K. Edlund, E. Lundberg, S. Navani, C. A.-K. Szigyarto, J. Odeberg, D. Djureinovic, J. O. Takanen, S. Hober, T. Alm, P.-H. Edqvist, H. Berling, H. Tegel, J. Mulder, J. Rockberg, P. Nilsson, J. M. Schwenk, M. Hamsten, K. von

Feilitzen, M. Forsberg, L. Persson, F. Johansson, M. Zwahlen, G. von Heijne, J. Nielsen, F. Pontén, Tissue-based map of the human proteome. *Science* **347**, 1260419 (2015).

5. Method of the Year 2024: spatial proteomics. *Nat. Methods* **21**, 2195–2196 (2024).

6. B. Ghoshal, F. Hikmet, C. Pineau, A. Tucker, C. Lindskog, DeepHistoClass: A Novel Strategy for Confident Classification of Immunohistochemistry Images Using Deep Learning. *Mol. Cell. Proteomics MCP* **20**, 100140 (2021).

7. A. Shariff, J. Kangas, L. P. Coelho, S. Quinn, R. F. Murphy, Automated Image Analysis for High-Content Screening and Analysis. *J. Biomol. Screen.* **15**, 726–734 (2010).

8. M. Karlsson, C. Zhang, L. Méar, W. Zhong, A. Digre, B. Katona, E. Sjöstedt, L. Butler, J. Odeberg, P. Dusart, F. Edfors, P. Oksvold, K. von Feilitzen, M. Zwahlen, M. Arif, O. Altay, X. Li, M. Ozcan, A. Mardonoglu, L. Fagerberg, J. Mulder, Y. Luo, F. Ponten, M. Uhlén, C. Lindskog, A single–cell type transcriptomics map of human tissues. *Sci. Adv.* **7**, eabh2169 (2021).

9. J. F. Reiter, M. R. Leroux, Genes and molecular pathways underpinning ciliopathies. *Nat. Rev. Mol. Cell Biol.* **18**, 533–547 (2017).

10. L. B. Pedersen, N. Jurisch-Yaksi, F. Schmid, S. T. Christensen, Cilia and Flagella. *Encycl. Cell Biol. Second Ed.* **3**, 164–188 (2023).

11. J. Wallmeier, K. G. Nielsen, C. E. Kuehni, J. S. Lucas, M. W. Leigh, M. A. Zariwala, H. Omran, Motile ciliopathies. *Nat. Rev. Dis. Primer* **6**, 1–29 (2020).

12. D. Narayan, S. N. Krishnan, M. Upender, T. S. Ravikumar, M. J. Mahoney, T. F. Dolan, A. S. Teebi, G. G. Haddad, Unusual inheritance of primary ciliary dyskinesia (Kartagener's syndrome). *J. Med. Genet.* **31**, 493–496 (1994).

13. M. R. Krawczyński, H. Dmeńska, M. Witt, Apparent X-linked primary ciliary dyskinesia associated with retinitis pigmentosa and a hearing loss. *J. Appl. Genet.* **45**, 107–110 (2004).

14. K. A. Despotes, M. A. Zariwala, S. D. Davis, T. W. Ferkol, Primary Ciliary Dyskinesia: A Clinical Review. *Cells* **13**, 974 (2024).

15. M. Fliegauf, T. Benzing, H. Omran, When cilia go bad: cilia defects and ciliopathies. *Nat. Rev. Mol. Cell Biol.* **8**, 880–893 (2007).

16. L. B. Pedersen, N. Jurisch-Yaksi, F. Schmid, S. T. Christensen, "Cilia and Flagella" in *Encyclopedia of Cell Biology (Second Edition)*, R. A. Bradshaw, G. W. Hart, P. D. Stahl, Eds. (Academic Press, Oxford, 2023; https://www.sciencedirect.com/science/article/pii/B9780128216187002091), pp. 164–188.

17. T. Ishikawa, "Structure of Motile Cilia" in *Macromolecular Protein Complexes IV: Structure and Function*, J. R. Harris, J. Marles-Wright, Eds. (Springer International Publishing, Cham, 2022; https://doi.org/10.1007/978-3-031-00793-4_15), pp. 471–494.

18. J. Gopalakrishnan, K. Feistel, B. M. Friedrich, A. Grapin-Botton, N. Jurisch-Yaksi, E. Mass, D. U. Mick, R. Müller, H. May-Simera, B. Schermer, M. Schmidts, P. Walentek, D. Wachten, Emerging principles of primary cilia dynamics in controlling tissue organization and function. *EMBO J.* **42**, e113891 (2023).

19. M. Fliegauf, H. Olbrich, J. Horvath, J. H. Wildhaber, M. A. Zariwala, M. Kennedy, M. R. Knowles, H. Omran, Mislocalization of DNAH5 and DNAH9 in Respiratory Cells from Patients with Primary Ciliary Dyskinesia. *Am. J. Respir. Crit. Care Med.* **171**, 1343–1349 (2005).

20. J. Awata, S. Takada, C. Standley, K. F. Lechtreck, K. D. Bellvé, G. J. Pazour, K. E. Fogarty, G. B. Witman, NPHP4 controls ciliary trafficking of membrane proteins and large soluble proteins at the transition zone. *J. Cell Sci.* **127**, 4714–4727 (2014).

21. M. Fliegauf, J. Horvath, C. von Schnakenburg, H. Olbrich, D. Müller, J. Thumfart, B. Schermer, G. J. Pazour, H. P. H. Neumann, H. Zentgraf, T. Benzing, H. Omran, Nephrocystin specifically localizes to the transition zone of renal and respiratory cilia and photoreceptor connecting cilia. *J. Am. Soc. Nephrol. JASN* **17**, 2424–2433 (2006).

22. P. G. Czarnecki, J. V. Shah, The ciliary transition zone: From Morphology and Molecules to Medicine. *Trends Cell Biol.* **22**, 201–210 (2012).

23. I. V. Nechipurenko, A. Olivier-Mason, A. Kazatskaya, J. Kennedy, I. G. McLachlan, M. G. Heiman, O. E. Blacque, P. Sengupta, A conserved role for Girdin in basal body positioning and ciliogenesis. *Dev. Cell* **38**, 493–506 (2016).

24. L. R. Bonser, B. W. Schroeder, L. A. Ostrin, N. Baumlin, J. L. Olson, M. Salathe, D. J. Erle, The Endoplasmic Reticulum Resident Protein AGR3. Required for Regulation of Ciliary Beat Frequency in the Airway. *Am. J. Respir. Cell Mol. Biol.* **53**, 536–543 (2015).

25. J. Wallmeier, D. Frank, A. Shoemark, T. Nöthe-Menchen, S. Cindric, H. Olbrich, N. T. Loges, I. Aprea, G. W. Dougherty, P. Pennekamp, T. Kaiser, H. M. Mitchison, C. Hogg, S. B. Carr, M. A. Zariwala, T. Ferkol, M. W. Leigh, S. D. Davis, J. Atkinson, S. K. Dutcher, M. R. Knowles, H. Thiele, J. Altmüller, H. Krenz, M. Wöste, A. Brentrup, F. Ahrens, C. Vogelberg, D. J. Morris-Rosendahl, H. Omran, De Novo Mutations in FOXJ1 Result in a Motile Ciliopathy with Hydrocephalus and Randomization of Left/Right Body Asymmetry. *Am. J. Hum. Genet.* **105**, 1030–1039 (2019).

26. Å. Sivertsson, E. Lindström, P. Oksvold, B. Katona, F. Hikmet, J. Vuu, J. Gustavsson, E. Sjöstedt, K. von Feilitzen, C. Kampf, J. M. Schwenk, M. Uhlén, C. Lindskog, Enhanced Validation of Antibodies Enables the Discovery of Missing Proteins. *J. Proteome Res.* **19**, 4766–4781 (2020).

27. C. M. Sadek, A. Jiménez, A. E. Damdimopoulos, T. Kieselbach, M. Nord, J.-Å. Gustafsson, G. Spyrou, E. C. Davis, R. Oko, F. A. van der Hoorn, A. Miranda-Vizuete, Characterization of Human Thioredoxin-like 2. *J. Biol. Chem.* **278**, 13133–13142 (2003).

28. M. Zariwala, W. K. O'Neal, P. G. Noone, M. W. Leigh, M. R. Knowles, L. E. Ostrowski, Investigation of the Possible Role of a Novel Gene, DPCD, in Primary Ciliary Dyskinesia. *Am. J. Respir. Cell Mol. Biol.* **30**, 428–434 (2004).

29. C. Maurizy, M. Quinternet, Y. Abel, C. Verheggen, P. E. Santo, M. Bourguet, A. C. F. Paiva, B. Bragantini, M.-E. Chagot, M.-C. Robert, C. Abeza, P. Fabre, P. Fort, F. Vandermoere, P. M. F. Sousa, J.-C. Rain, B. Charpentier, S. Cianférani, T. M. Bandeiras, B. Pradet-Balade, X. Manival, E. Bertrand, The RPAP3-Cterminal domain identifies R2TP-like quaternary chaperones. *Nat. Commun.* **9**, 2093 (2018).

30. Y.-Q. Mao, T. V. Seraphim, Y. Wan, R. Wu, E. Coyaud, M. B. Munim, A. Mollica, E. Laurent, M. Babu, V. Mennella, B. Raught, W. A. Houry, DPCD is a regulator of R2TP in ciliogenesis initiation through Akt signaling. *Cell Rep.* **43** (2024).

31. C. Dafinger, M. M. Rinschen, L. Borgal, C. Ehrenberg, S. G. Basten, M. Franke, M. Höhne, M. Rauh, H. Göbel, W. Bloch, F. T. Wunderlich, D. J. M. Peters, D. Tasche, T. Mishra, S. Habbig, J. Dötsch, R.-U. Müller, J. C. Brüning, T. Persigehl, R. H. Giles, T. Benzing, B. Schermer, M. C. Liebau, Targeted deletion of the AAA-ATPase Ruvbl1 in mice disrupts ciliary integrity and causes renal disease and hydrocephalus. *Exp. Mol. Med.* **50**, 1–17 (2018).

32. C. Coutton, G. Martinez, Z.-E. Kherraf, A. Amiri-Yekta, M. Boguenet, A. Saut, X. He, F. Zhang, M. Cristou-Kent, J. Escoffier, M. Bidart, V. Satre, B. Conne, S. Fourati Ben Mustapha, L. Halouani, O. Marrakchi, M. Makni, H. Latrous, M. Kharouf, K. Pernet-Gallay, M. Bonhivers, S. Hennebicq, N. Rives, E. Duliouist, A. Touré, H. Gourabi, Y. Cao, R. Zouari, S. H. Hosseini, S. Nef, N. Thierry-Mieg, C. Arnoult, P. F. Ray, Bi-allelic Mutations in ARMC2 Lead to Severe Astheno-Teratozoospermia Due to Sperm Flagellum Malformations in Humans and Mice. *Am. J. Hum. Genet.* **104**, 331–340 (2019).

33. B. Wu, W. Zhang, H. Yu, L. Ruan, K. Wang, M. Gu, H. Geng, J. Fang, C. Xu, Y. Sheng, Q. Tan, Q. Shen, Z. Duan, H. Wu, R. Hua, R. Guo, Z. Wei, P. Zhou, Y. Xu, Y. Cao, X. He, K. Li, M. Lv, D. Tang, Broadening the ARMC2 mutational phenotype: linking multiple morphological abnormalities of the Flagella to Pulmonary Manifestations in Primary Ciliary Dyskinesia. *Reprod. Biol. Endocrinol. RBE* **23**, 48 (2025).

34. Y. Liang, T. F. Tedder, Identification of a CD20-, FcεRIβ-, and HTm4-Related Gene Family: Sixteen New MS4A Family Members Expressed in Human and Mouse. *Genomics* **72**, 119–127 (2001).

35. W. Li, A. Mukherjee, J. Wu, L. Zhang, M. E. Teves, H. Li, S. Nambiar, S. C. Henderson, A. R. Horwitz, J. F. Strauss III, X. Fang, Z. Zhang, Sperm Associated Antigen 6 (SPAG6) Regulates Fibroblast Cell Growth, Morphology, Migration and Ciliogenesis. *Sci. Rep.* **5**, 16506 (2015).

36. M. E. Teves, P. R. Sears, W. Li, Z. Zhang, W. Tang, L. van Reesema, R. M. Costanzo, C. W. Davis, M. R. Knowles, J. F. Strauss, Z. Zhang, Sperm-Associated Antigen 6 (SPAG6)

Deficiency and Defects in Ciliogenesis and Cilia Function: Polarity, Density, and Beat. *PLoS ONE* **9**, e107271 (2014).

37. R. Sapiro, I. Kostetskii, P. Olds-Clarke, G. L. Gerton, G. L. Radice, J. F. Strauss III, Male Infertility, Impaired Sperm Motility, and Hydrocephalus in Mice Deficient in Sperm-Associated Antigen 6. *Mol. Cell. Biol.* **22**, 6298–6305 (2002).

38. T. Kanie, B. Liu, J. F. Love, S. D. Fisher, A.-K. Gustavsson, P. K. Jackson, A hierarchical pathway for assembly of the distal appendages that organize primary cilia. *eLife* **14**, e85999 (2025).

39. P. Radhakrishnan, N. Quadri, F. Erger, N. Fuhrmann, O.-M. Geist, C. Netzer, I. Khyriem, M. Muranjan, V. Udani, M. Yeole, S. Mascarenhas, S. Limaye, S. Siddiqui, P. Upadhyai, A. Shukla, Biallelic Variants in Impair Ciliogenesis and Cause a Severe Neurological Disorder. *Clin. Genet.* **107**, 311–322 (2025).

40. X. Liu, Y. Peng, J. Wang, Integrative analysis of DNA methylation and gene expression profiles identified potential breast cancer-specific diagnostic markers. *Biosci. Rep.* **40**, BSR20201053 (2020).

41. C. Lu, Y. Yang, L. Lingmei, H. Qiujuan, G. Qianru, Q. Lisha, C. Wenfeng, N. Yun, Z. peisen, Identification of hub genes in AR-induced tamoxifen resistance in breast cancer based on weighted gene co-expression network analysis. *Breast Cancer Res. Treat.* **197**, 71–82 (2023).

42. S. Henriksson, H. Rassoolzadeh, E. Hedström, C. Coucoravas, A. Julner, M. Goldstein, G. Imreh, B. Zhivotovsky, M. B. Kastan, T. Helleday, M. Farnebo, The scaffold protein WRAP53β orchestrates the ubiquitin response critical for DNA double-strand break repair. *Genes Dev.* **28**, 2726–2738 (2014).

43. A. Wilken, I. M. Höben, A. Wolter, N. T. Loges, H. Olbrich, I. Aprea, B. Dworniczak, J. Raidt, H. Omran, Primary Ciliary Dyskinesia Associated Disease-Causing Variants in CCDC39 and CCDC40 Cause Axonemal Absence of Inner Dynein Arm Heavy Chains DNAH1, DNAH6, and DNAH7. *Cells* **13**, 1200 (2024).

44. T. Walton, M. Gui, S. Velkova, M. R. Fassad, R. A. Hirst, E. Haarman, C. O'Callaghan, M. Bottier, T. Burgoyne, H. M. Mitchison, A. Brown, Axonemal structures reveal mechanoregulatory and disease mechanisms. *Nature* **618**, 625–633 (2023).

45. J. Neesen, M. R. Koehler, R. Kirschner, C. Steinlein, J. Kreutzberger, W. Engel, M. Schmid, Identification of dynein heavy chain genes expressed in human and mouse testis: chromosomal localization of an axonemal dynein gene. *Gene* **200**, 193–202 (1997).

46. P. Sampaio, R. R. Ferreira, A. Guerrero, P. Pintado, B. Tavares, J. Amaro, A. A. Smith, T. Montenegro-Johnson, D. J. Smith, S. S. Lopes, Left-Right Organizer Flow Dynamics: How Much Cilia Activity Reliably Yields Laterality? *Dev. Cell* **29**, 716–728 (2014).

47. P. Legrain, R. Aebersold, A. Archakov, A. Bairoch, K. Bala, L. Beretta, J. Bergeron, C. H. Borchers, G. L. Corthals, C. E. Costello, E. W. Deutsch, B. Domon, W. Hancock, F. He, D. Hochstrasser, G. Marko-Varga, G. H. Salekdeh, S. Sechi, M. Snyder, S. Srivastava, M. Uhlén, C. H. Wu, T. Yamamoto, Y.-K. Paik, G. S. Omenn, The Human Proteome Project: Current State and Future Direction. *Mol. Cell. Proteomics MCP* **10**, M111.009993 (2011).

48. G. S. Omenn, S. Orchard, L. Lane, C. Lindskog, C. Pineau, C. M. Overall, B. Budnik, J. M. Mudge, N. H. Packer, S. T. Weintraub, M. H. A. Roehrl, E. Nice, T. Guo, J. E. Van Eyk, U. Völker, G. Zhang, N. Bandeira, R. Aebersold, R. L. Moritz, E. W. Deutsch, The 2024 Report on

the Human Proteome from the HUPO Human Proteome Project. *J. Proteome Res.* **23**, 5296–5311 (2024).

49. A. Kobayashi, K. Kawaguchi, S. Asano, H. Wu, T. Nakano, T. Inui, Y. Marunaka, T. Nakahari, The Increase in the Frequency and Amplitude of the Beating of Isolated Mouse Tracheal Cilia Reactivated by ATP and cAMP with Elevation in pH. *Int. J. Mol. Sci.* **25**, 8138 (2024).

50. J. L. Rosenbaum, G. B. Witman, Intraflagellar transport. *Nat. Rev. Mol. Cell Biol.* **3**, 813–825 (2002).

51. F. Hildebrandt, T. Benzing, N. Katsanis, Ciliopathies. *N. Engl. J. Med.* **364**, 1533–1543 (2011).

52. C. Kampf, I. Olsson, U. Ryberg, E. Sjöstedt, F. Pontén, Production of Tissue Microarrays, Immunohistochemistry Staining and Digitalization Within the Human Protein Atlas. *J. Vis. Exp. JoVE*, 3620 (2012).

53. J. Schindelin, I. Arganda-Carreras, E. Frise, V. Kaynig, M. Longair, T. Pietzsch, S. Preibisch, C. Rueden, S. Saalfeld, B. Schmid, J.-Y. Tinevez, D. J. White, V. Hartenstein, K. Eliceiri, P. Tomancak, A. Cardona, Fiji: an open-source platform for biological-image analysis. *Nat. Methods* **9**, 676–682 (2012).

54. 廖炳松, 陳澤生, 詹寶珠, A Fast Algorithm for Multilevel Thresholding. *J. Inf. Sci. Eng.* **17**, 713–727 (2001).

55. HPP Portal. https://hppportal.net/.
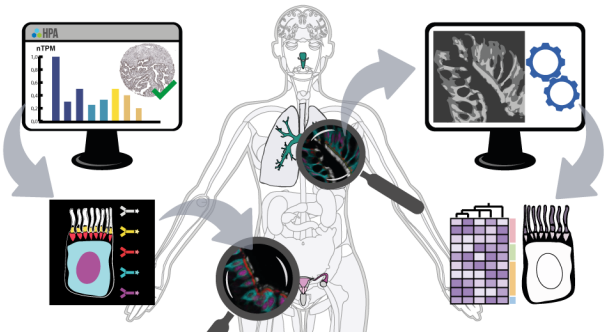
GRAPHICAL ABSTRACT